



# Effect of structural disorder induced by external irradiation with heavy ions on the alteration of a four oxide borosilicate glass

Stéphane Gin, Mélanie Taron, Hélène Arena, Jean-Marc Delaye

## ► To cite this version:

Stéphane Gin, Mélanie Taron, Hélène Arena, Jean-Marc Delaye. Effect of structural disorder induced by external irradiation with heavy ions on the alteration of a four oxide borosilicate glass. *npj Materials Degradation*, 2024, 8 (1), pp.64. 10.1038/s41529-024-00483-5 . cea-04737668

**HAL Id: cea-04737668**

**<https://cea.hal.science/cea-04737668v1>**

Submitted on 15 Oct 2024

**HAL** is a multi-disciplinary open access archive for the deposit and dissemination of scientific research documents, whether they are published or not. The documents may come from teaching and research institutions in France or abroad, or from public or private research centers.




L'archive ouverte pluridisciplinaire **HAL**, est destinée au dépôt et à la diffusion de documents scientifiques de niveau recherche, publiés ou non, émanant des établissements d'enseignement et de recherche français ou étrangers, des laboratoires publics ou privés.



Distributed under a Creative Commons Attribution 4.0 International License

<https://doi.org/10.1038/s41529-024-00483-5>

# Effect of structural disorder induced by external irradiation with heavy ions on the alteration of a four oxide borosilicate glass

Stéphane Gin  , Mélanie Taron, Hélène Arena  & Jean-Marc Delaye

The irradiation of glass by heavy ions induces structural damage, generally leading to a decrease in its chemical durability whose amplitude strongly depends on the glass chemical composition. Here, we investigate the effects of irradiation by 7 MeV Au ions (simulating the main ballistic effects induced by self-irradiation in nuclear glass) on the behavior of a 4-oxide borosilicate glass in both the initial and residual dissolution regimes. The comparison between irradiated and non-irradiated glasses provides insights into the predominant atomic mechanisms governing glass alteration processes. The most pronounced effect is observed on interdiffusion in acidic conditions, with the rate increased by more than an order of magnitude for the irradiated glass. We show that both the interdiffusion regime and the residual regime are controlled by the hydrolysis of the B—O—Si linkages, whereas under initial dissolution rate regime in basic conditions the rate-limiting step becomes the hydrolysis of Si—O—Si linkages. Overall, the observations suggest structural disorder due to external irradiation by Au ions primarily affects the kinetics of glass alteration without changing the fundamental nature of the limiting reactions.

In many countries, fission products from used nuclear fuels are confined in borosilicate glasses<sup>1–3</sup>. Due to their hazardous nature, these materials are intended for deep geological disposal. It is established that the release of radionuclides into the environment would primarily result from the action of water<sup>4</sup>. Water alters the glass through processes involving ion exchange and hydrolysis of chemical bonds forming the glass network<sup>5</sup>. The literature extensively covers this field, with several recent reviews summarizing the state of knowledge<sup>6,7</sup>. Overall, it is established that a borosilicate nuclear glass in contact with water undergoes first initial dissolution at a rate controlled by the hydrolysis of the glass network without feedback from elements released into the solution. This is followed by a residual dissolution rate regime controlled by the decreasing affinity of the dissolution reaction due to the increased concentrations in the solution of dissolved glass elements and the formation of a passivating layer limiting the transport of elements between the glass and the solution. The generally amorphous passivating layer can be destabilized by the precipitation of secondary phases, potentially leading to a resumption of glass alteration<sup>4,8</sup>.

The initial rate, characterized by a linear release of Si into solution in a very diluted solution, is preceded by faster reactions called interdiffusion or ion-exchange corresponding to both interactions between hydrogenated species and elements acting as glass modifier, and B hydrolysis<sup>5,9</sup>. The preponderance of these reactions depend on the nonbridging oxygen

(NBO) content of the glass and the pH. The more acidic the pH, the more intense these exchange reactions are<sup>10</sup>. This release of glass components follows a square root of time dependency, unlike the hydrolysis of the silicate network, which remains constant as long as the solution remains diluted. The mechanisms controlling the residual rate are still debated and seem to depend on the glass composition, alteration conditions (pH, solution composition), and the progress of the reaction<sup>11</sup>. It might be the rate of water diffusion in glass triggering ion-exchange reaction<sup>12</sup>, or of B hydrolysis from the silicate network or the transport of dissolved species through the gel or the precipitation of secondary phases<sup>11</sup>.

This mechanistic knowledge primarily results from studies on non-radioactive glasses used as surrogate for nuclear glasses. The effects of self-irradiation on glass alteration have also been studied but to a lesser extent. It is established that self-irradiation modifies the glass structure<sup>13–15</sup>. The main structural damage in nuclear glasses is due to recoil nuclei from alpha emitters<sup>16</sup>. They are of ballistic and electronic nature, leading to a slight variations in glass density<sup>17</sup>, a decrease in boron coordination, an increase in hardness, and fracture toughness<sup>18</sup>. These effects can be simulated by external irradiations with heavy ions, although it is not possible to reproduce exactly the effects of self-irradiation by fission products and minor actinides contained in nuclear glass using a single and unidirectional external irradiation<sup>19</sup>. For borosilicate glasses irradiated with heavy ions, an increase

CEA, DES, ISEC, DPME, SEME, University of Montpellier, Marcoule, Montpellier F-30207 Bagnols-sur-Cèze, France.

 e-mail: [stephane.gin@cea.fr](mailto:stephane.gin@cea.fr)

in interdiffusion rate<sup>20</sup> and initial dissolution rate has been observed in some cases<sup>21–24</sup>, whereas no measurable effects have been reported in some other cases<sup>14,25</sup>. However, it seems that the simpler the glass, the more pronounced the effects of irradiation on the initial dissolution rate. Regarding the residual regime, it seems that the alpha dose increases the amount of altered glass in this regime<sup>26,27</sup>. When structural disorder within the glass is obtained through fast quenching, a slight increase of both the initial dissolution rate and the residual rate are also observed<sup>28</sup>. Although hypotheses have been made, the origin of these effects is not yet well understood, justifying more investigations related to the impacts of structural changes within the glass to the mechanisms of alteration.

In this study, we chose a 4-oxide borosilicate glass (CJ2 glass). It is a simplified version of the International Simple Glass (ISG) glass from which Ca and Zr have been removed<sup>29</sup>. This glass serves as a good model for more complex glasses, such as SON68<sup>30</sup>. A defining feature of this glass is its low concentration of non-bridging oxygen (NBO), approximately 0.037 per tetrahedron of Si + Al. This indicates that sodium essentially serves as a charge compensator for both  $\text{BO}_4^-$  and  $\text{AlO}_4^-$  units. The CJ2 glass was irradiated with 7 MeV Au ions at a fluence of  $2 \times 10^{14}$  at/cm<sup>2</sup>, impacting the first two microns of the material. The corresponding dose is above that required to induce the maximum structural changes within the glass<sup>19</sup>. The aqueous alteration of this glass was studied by comparing it to that of a non-irradiated CJ2 glass specimen. The study focuses on the initial regime by conducting an experiment favoring interdiffusion (low temperature and acidic pH) and measuring the initial dissolution rate of the glass at 90°C and pH 9. It also examines the residual regime from an experiment conducted in a solution close to saturation with respect to amorphous silica and enriched in  $\text{H}_2^{18}\text{O}$ , also carried out at 90°C and pH 9. Overall, this study shows a pronounced effect of pre-irradiation on interdiffusion, which, for this glass, involves Si–O–B bonds breaking along with the exchange reaction between  $\text{H}_3\text{O}^+$  and  $\text{Na}^+$ . The connection between these results and those obtained for initial and residual rates, on irradiated and non-irradiated glasses, is discussed to improve the understanding of the atomistic phenomena that control the main alteration mechanisms of nuclear glasses.

## Results

### Glass structure

Figure 1 shows the Raman spectra of the non-irradiated and Au-irradiated CJ2 glasses. The main changes observed between the spectra of the non-irradiated and irradiated glasses are the evolution in the R-band and the evolution of the  $\text{Q}^n$  band. The R-band, around 480 cm<sup>-1</sup>, is representative of the bending and rocking modes of Si–O–Si bonds. A shift of 10 cm<sup>-1</sup> towards higher wavelengths is seen on the irradiated glass, corresponding to a decrease in the average Si–O–Si angle<sup>31</sup>. The  $\text{Q}^n$  band (850–1200 cm<sup>-1</sup>) is associated with the connectivity between  $\text{SiO}_4$  tetrahedra. Between the non-irradiated and irradiated glass, an increase in the band intensity at shorter wavelengths is observed, indicating a depolymerization of the silicate network in irradiated glass compared to nonirradiated glass<sup>32,33</sup>. The spectrum of the irradiated glass shows an increase in the intensity of the D2 band (600 cm<sup>-1</sup>) compared to the spectrum of the non-irradiated glass, which is tied to three-membered rings of  $\text{SiO}_4$ <sup>34</sup>. This indicates a broadening in the distribution of the silicate network rings in irradiated glass, with, in particular, an increase in the number of 3-membered rings. Such changes have been reported to a much lower extent on complex glasses under irradiation<sup>19,35</sup>. The intensity of the band at 770 cm<sup>-1</sup> is modified between the two spectra, which is attributed to six-membered rings with at least one  $\text{BO}_4^-$  unit and boroxol rings<sup>34</sup>. It indicates a change in the distribution of borate rings between irradiated and non-irradiated glass and possibly a diminution of the population of four-coordinated boron ( $\text{B}^{\text{IV}}$ ). This result is expected when comparing these data to those obtained on ISG glass subjected to the same irradiation<sup>35</sup>. Indeed, through NMR spectroscopy, it has been shown that the 50%  $\text{B}^{\text{IV}}$  fraction for the non-irradiated glass dropped to 36% for the glass irradiated with 7 MeV Au ions at a fluence of  $2 \times 10^{14}$  at/cm<sup>2</sup>. A similar

variation can be anticipated in our case, given the resemblance between CJ2 and ISG. Such a variation in B speciation would increase NBOs from 0.037 to 0.1 per Si and Al tetrahedra.

Finally, the band between 1300 and 1550 cm<sup>-1</sup>, representative of the stretching of B–O bonds of  $\text{BO}_3$  species<sup>18</sup>, increases in intensity for the irradiated glass compared to the non-irradiated glass, towards the highest wavelengths. As the band at 1450 cm<sup>-1</sup> is associated with the presence of  $\text{BO}_3$  linked to NBO<sup>18</sup>, it seems that irradiation with Au ions leads to a change in the proportion of  $\text{BO}_3/\text{BO}_4^-$  with an increase in tri-coordinated boron ( $\text{B}^{\text{III}}$ ) and the number of NBO. These modifications are also consistent with the results obtained by Gin et al.<sup>33</sup> on a CJ2 glass irradiated with Xe 1 GeV. The structural damage caused by 7 MeV Au irradiation appears less important than with 1 GeV Xe, according to variations of the Raman peaks intensity<sup>33</sup>. Furthermore, high energy ions such as 1 GeV Xe could form ion tracks in the glass, making the material more sensitive to aqueous alteration<sup>19</sup>. It is worth noting that in actual radioactive glass, ion tracks do not form because alpha emitters do not have sufficient energy<sup>36</sup>.

### Interdiffusion rate

The experiments aimed at studying interdiffusion were conducted at a temperature of 30°C using polished monoliths placed in a solution with pH adjusted to 1. Note that a concentration of  $\sim 10^{-4}$  M of KCl was added to the solution in order to use K as an exogenous tracer for the ToF-SIMS analyses. For each glass (non-irradiated and irradiated), one monolith was removed after 8 hours, and the other after 3 days. The altered layers were analyzed by ToF-SIMS. The solution was analyzed by ICP-OES after 3 days of experiment to confirm the dominance of interdiffusion over the hydrolysis of the silicate network.

Solution data provide information only for irradiated CJ2 after 3 days of alteration. Before that leaching time the elemental concentrations were below detection limits. Nonetheless, this analysis shows that both Na and B give an equivalent thickness of altered glass of  $1.1 \pm 0.1$  μm and a concentration of Si below the detection limit ( $< 0.1$  ppm), which corresponds to a dissolved thickness  $< 2$  nm, confirming that dissolution of the silicate network is negligible in the tested conditions.

Figure 2 shows the results of the ToF-SIMS analyses conducted after 8 hours (subfigures a and b) and 3 days (subfigures c and d). First of all, in all cases, it can be noticed that glass alteration is characterized by a depletion of Al, B and Na. The depletion front of the 3 elements increases in the order of Al, B and Na.

For the non-irradiated samples, the potassium signal has a Gaussian shape with full width at half maximum (FWHM) of 10 nm after 8 hours and 15 nm after 3 days. For the irradiated sample altered 8 hours the FWHM is 30 nm. For the 3-day sample, potassium does not exhibit a well-defined peak, which is why the profile is not shown. The width of the K peak is indicative of interface roughness<sup>37</sup>. As K, being an exogenous element, diffuses from the solution into the alteration layer but does not diffuse into the pristine glass<sup>38</sup>, we chose to place the alteration front at the maximum of the potassium peak. Thus, for the non-irradiated glass, the alteration layer has a thickness of 18 nm and is depleted in Al by about 5 nm. After 3 days, the alteration layer measures 38 nm, and the thickness of the Al-depleted zone has not changed. The gap between the Na and B fronts is approximately 10 nm for both time points, measured at half-height of the profiles. Finally, the profile of H is anticorrelated with those of B and Na. For the irradiated samples, the alteration layer has a thickness of 145 nm after 8 hours and 1300 nm after 3 days. For these two samples, the Al-depleted outer layer is thin ( $\sim 10$  nm) and similar at the two durations. Moreover, the shift between Na and B profile is not visible, suggesting that, if it exists, it is small and probably close to that of the non-irradiated samples.

As a whole, this experiment highlights a large increase of interdiffusion phenomenon for the irradiated sample compared to the reference (x8 after 8 hours and x34 after 3 days). Despite slight difference in the position of B and Na depletion front, the behavior of the two elements remain very similar

whatever the duration and the glass state (non-irradiated or irradiated). In the recent literature, interdiffusion in sodium silicate glass covers various reactions, including water diffusion, exchange between protons from water molecule with sodium but also the formation of silanols and condensation between adjacent silanols<sup>39</sup>. In borosilicate glass, more processes are at play as B is also leached out of the glass in acidic conditions. Because activation energy for B—O—Si breaking is higher than that for Na<sup>+</sup> dissociation from Si—O<sup>−</sup> or <sup>IV</sup>B—O<sup>−</sup><sup>5,40</sup>, the almost congruent B and Na release in our

experiments implies that the release of B is the rate-limiting step. Thus, the hydrolysis of B allows water diffusion in the solid and ion exchange to occur. This is in line with previous results with ISG<sup>10,11</sup> and probably due to the low fraction of NBO in our glass (0.037 per Si and Al tetrahedra), preventing a preferential release of Na through percolation channels<sup>41</sup>.

### Initial dissolution rate

The experiments for measuring the initial dissolution rate were conducted in parallel, in static mode with a solution stirred by a magnetic bar, using polished monoliths at a temperature of 90°C and pH 9 adjusted with a LiOH solution<sup>42</sup>. Figure 3 illustrates the evolution of normalized mass losses for the 4 cations of CJ2 glass (tabulated data are provided in Supplementary Information 2). At the end of the measurement, the dissolved glass thickness for the irradiated sample is 1.4 μm, which is less than the irradiated zone (2 μm). Thus, the measurement accurately targeted the irradiated area.

The dissolution curves are linear since the beginning of the experiments. Within uncertainties, for each experiment, the dissolution rate of the 4 elements of the glass is similar, indicating congruence in the dissolution of both non-irradiated and irradiated CJ2 glass. Initial dissolution rates,  $r_{0,non-irr}$  and  $r_{0,irr}$  were calculated from Si release into the solution according to Eq. 4. The initial dissolution rate of irradiated CJ2 glass ( $10.9 \pm 3.3 \text{ g}\cdot\text{m}^{-2}\cdot\text{d}^{-1}$ ) is 2.3 times higher than that of non-irradiated reference glass ( $4.7 \pm 1.4 \text{ g}\cdot\text{m}^{-2}\cdot\text{d}^{-1}$ ). The uncertainty in these rates is 30%, as suggested in a previous study on ISG glass<sup>43</sup>. This effect of irradiation on initial dissolution rate is in line with previous studies conducted on simple borosilicate glasses, showing an increase of the rate related to the structural changes induced by irradiation<sup>21,24,44</sup>.

### Residual rate

The residual dissolution rate of glass was studied at 90°C and pH 9 through a static mode experiment in a solution close to saturation with respect to

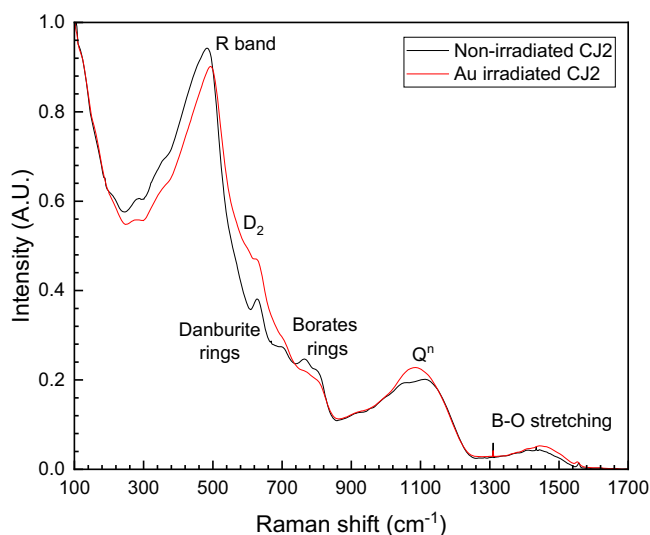


**Fig. 1** | Normalized Raman spectra of the non-irradiated and Au-irradiated CJ2 glasses.

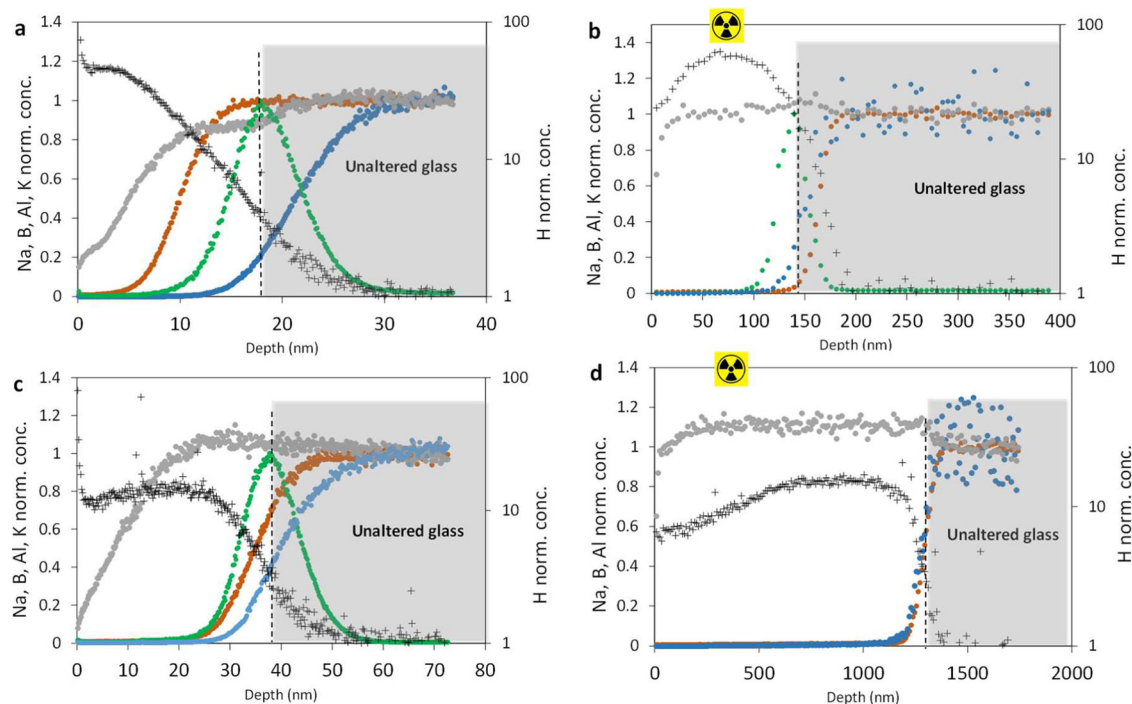


**Fig. 2** | ToF-SIMS profiles of glass samples altered at 30°C pH 1. **a** and **b** correspond to profiles after 8 hours of alteration for non-irradiated and irradiated samples, respectively, whereas **c** and **d** correspond to 3 days of alteration for non-irradiated and irradiated sample, respectively. Na, B, and Al intensities were normalized first to that of Si and then to pristine glass. This double normalization better highlights the behavior of Al. H intensity was normalized to that in pristine glass (which mostly corresponds to the background signal provided by the low air

pressure in the chamber). K intensity was normalized to the maximum intensity recorded. It was verified by solution analysis that Si was not dissolved during this experiment, meaning that Si concentration in the alteration layer is constant. These figures highlight the depletion of Al in the outer region of the alteration layer, the position of the alteration front thanks to the peak of K, and the shift between B and Na profiles.

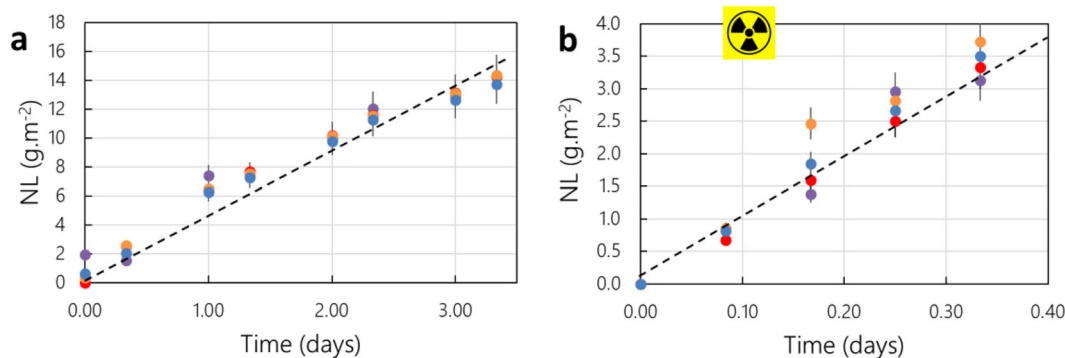


**Fig. 3 | Initial dissolution rate determined at 90°C and pH 9. a** Non-irradiated glass, **b** Irradiated glass. Note that although the experiment ran until 1.3 days, we consider only the first 0.4 day for the calculation of  $r_0$ . Indeed, beyond 0.4 day, the trend is no longer linear. The dashed lines serve as a visual guide. Relative uncertainty on NL is  $\pm 10\%$ .

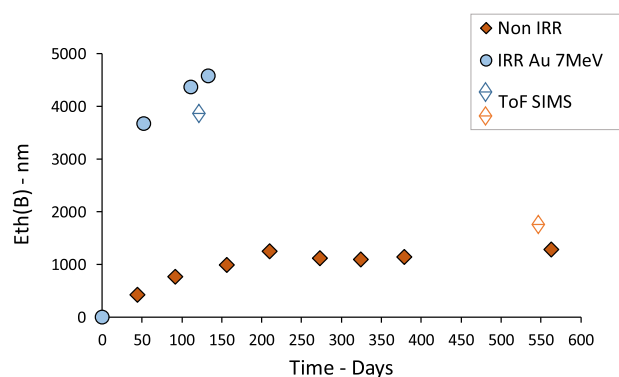


**Fig. 4 | Time evolution of altered glass thickness for the static experiment conducted in silica-saturated solution at 90°C and pH 9. Gel thickness obtained by ToF-SIMS are shown for comparison.**

amorphous silica. B was used as a tracer for glass alteration. Figure 4 presents the evolution of equivalent thickness of altered glass calculated from the release of B in solution for both non-irradiated and irradiated glass (tabulated data are provided in Supplementary Information 3). It appears that irradiated glass altered more in this regime compared to non-irradiated glass. The latter exhibits a first stage lasting approximately 200 days, during which the alteration increases slowly, followed by a cessation of alteration or an evolution below the measurement threshold. For irradiated glass, the alteration increases until 133 days. The experiment was terminated at day 133 as the altered thickness exceeded the thickness of the irradiated zone, namely 2  $\mu\text{m}$ .

Since both samples were altered in a solution of same composition, i.e. close to saturation with respect to amorphous silica, it is expected according to a previous study using  $^{29}\text{Si}$  as a probe to quantify the reactivity of the silicate network that the hydrolysis rate of Si-O-Si bonds is minimum in both cases<sup>45</sup>. The difference in behavior between the irradiated glass and the non-irradiated sample would then be solely attributed to both the rate of gel formation and their passivating properties. To delve deeper, characterizations of the gels were performed using ToF-SIMS.

Figure 5 presents the chemical profiles for the non-irradiated glass altered for 563 days. The transition between the gel and the pristine glass is marked by a significant decrease in the intensity of the H signal, anticorrelated with the signals of B and Na. The thickness of the gel layer ( $1.5 \pm 0.15 \mu\text{m}$ ) is in fairly good agreement with the thickness of the altered glass deduced from the solution analysis ( $1.1 \pm 0.55 \mu\text{m}$ ). It is important to note that the uncertainty in the thickness derived from ToF-SIMS is mainly associated with the assumption of an identical abrasion rate between the gel and the pristine glass. Meanwhile, the uncertainty in the calculated thickness from the solution analysis arises from the estimation of the reactive surface

and the analysis of the B concentration in the solution. These results are in line with previous studies showing that in the tested conditions C/J2 glass alters forming only a gel layer that replace the glass keeping constant the volume occupied by the solids<sup>30,33,44,46</sup>.

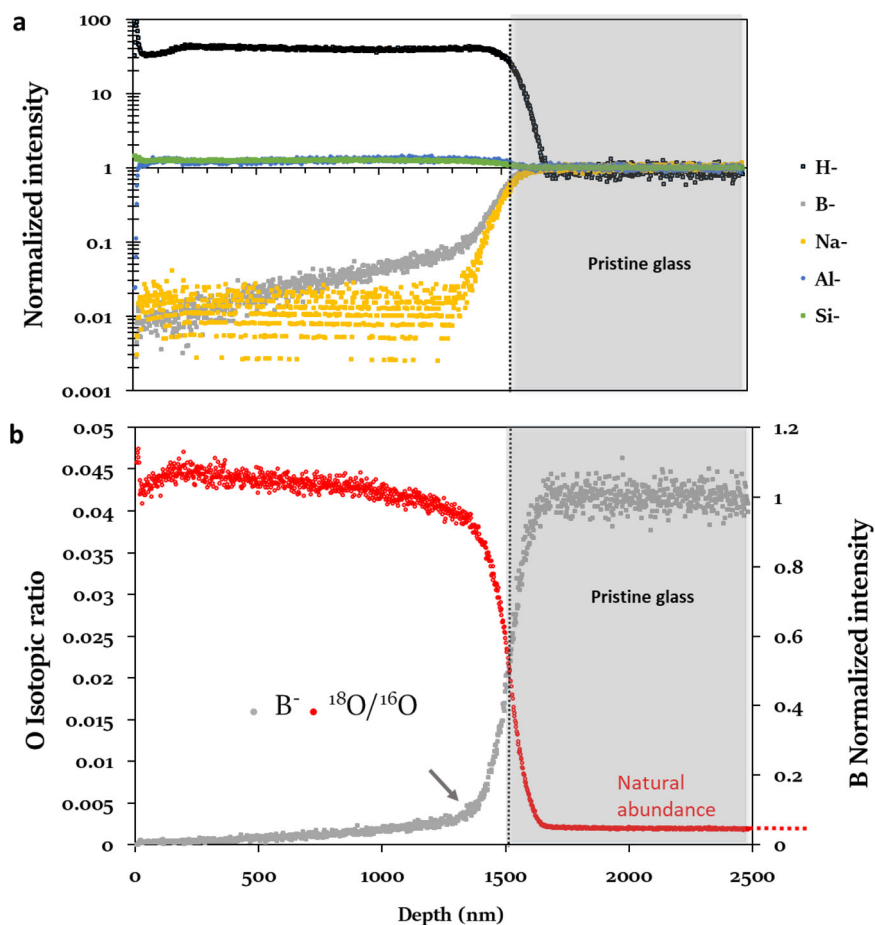
The intensity of Si and Al is similar in both the glass and the gel, which was expected according to the composition of the onset solution. Since the leaching solution is enriched in  $^{18}\text{O}$ , it appears that the gel incorporates O from water into its structure. The  $^{18}\text{O}$  can exist in the form of molecular water in the porosity, silanol groups, or as bridging oxygen between Si or Al tetrahedra. Given that the sample was rinsed with pure water ( $^{18}\text{O}/^{16}\text{O}$  at natural abundance) and analyzed under low-pressure conditions favorable to pore water evaporation, it is likely that  $^{18}\text{O}$  is primarily in the form of bridging oxygens and silanols. Overall, the isotopic ratio  $^{18}\text{O}/^{16}\text{O}$  in the gel is approximately half that of the solution. This indicates that a significant fraction of the bridging bonds forming the glass has been hydrolyzed by water molecules, but there still remains a non-negligible fraction of non-hydrolyzed bonds inherited from the glass. The shape of  $^{18}\text{O}/^{16}\text{O}$  profile is slightly decreasing toward the pristine glass, with a sharp decrease in the interfacial area between the gel and the pristine glass, as the glass has the isotopic signature of natural abundance. The decreasing slope could indicate the rate at which the gel undergoes hydrolysis/condensation reactions involving water molecules. Indeed, the external gel was the first to form, while the interfacial zone was the last to react. The profile of  $^{18}\text{O}/^{16}\text{O}$  in the gel is thus linked to the duration of gel maturation. This point is discussed after the results obtained for the irradiated sample.

Figure 6 presents ToF-SIMS profiles of the pre-irradiated sample after 133 days of alteration. Qualitatively, the profiles in H, Si, Al, B, and Na are similar to those of the non-irradiated glass, except for the significantly greater depth of alteration ( $3.8 \pm 0.4 \mu\text{m}$ ), in reasonable agreement with the solution analyses ( $4.5 \pm 0.9 \mu\text{m}$ ). Gold ions are detected up to  $2.1 \pm 0.2 \mu\text{m}$ , consistent with SRIM calculations ( $2 \mu\text{m}$ ) (Supplementary Information 1). Beyond this depth, it can be estimated that the glass exhibits the same structure as the non-irradiated glass. If this is the case, the non-irradiated glass zone would have been altered like the non-irradiated sample, around  $1.1 \mu\text{m}$  maximum, as shown by the solution data (Fig. 4). However, it is altered over  $1.8 \mu\text{m}$ , a thickness significantly greater than the measured gel thickness on the non-irradiated glass. Either there are still some modifications of the glass structure beyond  $2 \mu\text{m}$  making this zone more reactive than the unirradiated sample, or the gel formed from the  $2 \mu\text{m}$  irradiated glass may influence the ongoing alteration of the glass. The second hypothesis is more likely according to previous work on mechanical stress induced by the gel on the pristine glass surface<sup>47</sup>. Further examination is required to understand this result.

Compared to the non-irradiated sample, the gel of the pre-irradiated glass is more enriched in  $^{18}\text{O}$  and the decreasing slope of  $^{18}\text{O}/^{16}\text{O}$  is more pronounced than in the control sample ( $\frac{\Delta(^{18}\text{O}/^{16}\text{O})}{t} = 7 \times 10^{-5} \text{ d}^{-1}$  vs  $5 \times 10^{-6} \text{ d}^{-1}$ ) suggesting that the gel formed on the irradiated sample undergoes more



**Fig. 5 | ToF-SIMS profiles for the non-irradiated sample altered 563 days in the residual rate regime (silica saturated solution, 90°C, pH 9).** **a.** Si, Al, B, Na and H profiles in Log scale. **b.**  $^{18}\text{O}/^{16}\text{O}$  and B profiles in linear scale.  $^{18}\text{O}/^{16}\text{O}$  isotopic ratio of the starting solution is 0.098. B retention in the interfacial region of the gel is given by the change in the slope point marked by the grey arrow (10% of the glass concentration).



hydrolysis/condensation reactions. Besides, the gel zone beyond 2  $\mu\text{m}$  exhibits a decreasing but still slightly higher  $^{18}\text{O}/^{16}\text{O}$  isotopic ratio than the control sample (0.051  $\rightarrow$  0.045 vs 0.044  $\rightarrow$  0.040), confirming that this zone is more reactive than the non-irradiated glass.

Based on kinetic data and ToF-SIMS profiles, we calculated the value of the  $^{18}\text{O}/^{16}\text{O}$  isotopic ratio in the gel as a function of its actual contact time with the solution (referred to here as the gel maturation time) (Fig. 7). It is evident that the gel formed on the irradiated glass exhibits a much faster  $^{18}\text{O}$  incorporation kinetics compared to that of the non-irradiated glass.

Finally, it is worth noting a slightly lower retention of B in the gel for the irradiated glass than for the control glass (5% vs 10%), strongly suggesting that the gel formed on non-irradiated sample is more passivating.

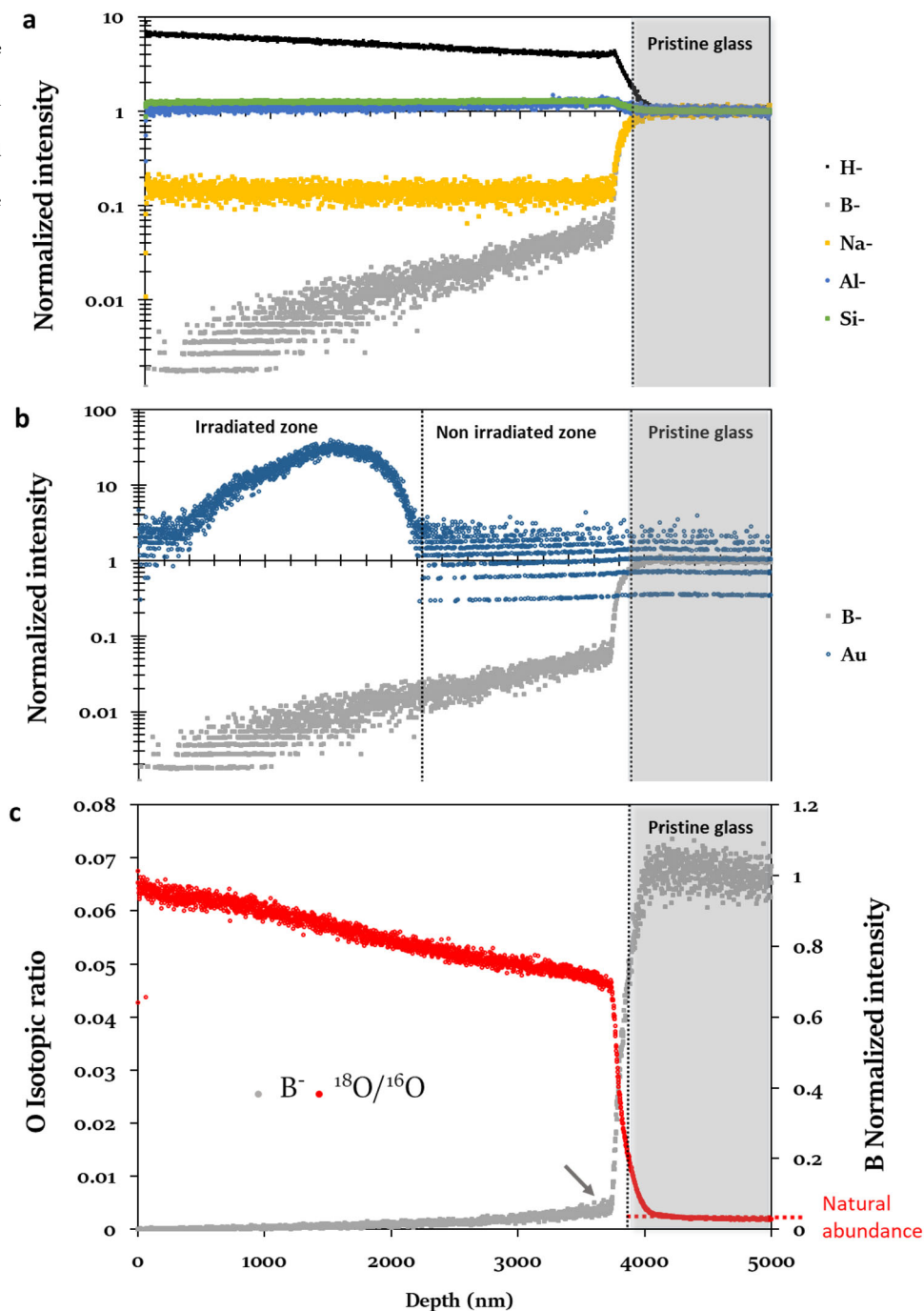
The two samples previously analyzed then underwent a tracing experiment (24 hours in a solution doped with  $^{10}\text{B}$  and  $^{18}\text{O}$ ) before a new ToF-SIMS analysis in cryogenic mode was made. The cryogenic mode is used to preserve as much as possible the pore water during the analysis. Figure 8 shows the isotopic profiles of O and B. The gel thicknesses are similar to those determined before tracing, evidence that the tracing experiment did not lead to a resumption of alteration. Next, a slight increase in the  $^{18}\text{O}/^{16}\text{O}$  ratio is observed in both samples after tracing, with a more pronounced difference in the outer zone of the gel formed on the non-irradiated glass. The isotopic ratio of B is similar in both gels and clearly indicates that the  $^{10}\text{B}$  introduced by the tracing solution does not penetrate up to the interface with the pristine glass, unlike  $^{18}\text{O}$ . In both cases,  $^{10}\text{B}$  is enriched in the first 300–400 nm of the gel. The slow diffusivity of B was already observed in tracing experiments. For instance, Damodaran et al (2022) reported apparent diffusion coefficient of B within ISG gel of the order of  $10^{-21} \text{ m}^2 \cdot \text{s}^{-1}$ <sup>48</sup>. The speciation of B in gel is not well known, although a former study suggested that B is likely under aqueous form<sup>49</sup>.

## Discussion

The experiments conducted in this study reveal a distinct behavior between the pre-irradiated CJ2 glass and the non-irradiated control glass. Regardless of the conditions, the irradiated glass shows more alteration than the control glass. However, the observed differences strongly depend on the alteration conditions. Indeed, the most significant difference was observed under low-temperature and acidic pH conditions, favoring interdiffusion. In this case, the almost congruent dissolution of B and Na is increased by more than an order of magnitude. Such an effect had not been reported in the literature to our knowledge. Congruence between B and Na indicates that breaking the B–O–Si bonds is necessary to allow the release of Na atoms into solution. The reason why interdiffusion is accelerated could have several potential causes, possibly additive. One is the swelling of the glass under irradiation. Although the density of irradiated CJ2 has not been measured, swelling should be close to that measured for ISG under same 7 MeV Au irradiation, 1.7%<sup>24</sup>. As swelling increases free volumes within the glass<sup>50</sup>, it can be hypothesized that  $\text{H}^+$  and  $\text{H}_2\text{O}$  diffusion is accelerated. This was for instance clearly demonstrated when comparing water diffusion in quartz ( $d = 2.68 \text{ g} \cdot \text{cm}^{-3}$ ) and silica glass ( $d = 2.28 \text{ g} \cdot \text{cm}^{-3}$ ), two  $\text{SiO}_2$  polymorphs with no NBO<sup>51</sup>. Another cause is the higher proportion of  $\text{B}^{\text{III}}$  in the irradiated glass. Since  $\text{B}^{\text{III}}$  dissolves faster than  $\text{B}^{\text{IV}}$ <sup>52</sup>, water diffusion in irradiated glass along with ion exchange are accelerated. Last, the stored energy within the irradiated glass is higher than in the reference glass making it more prone to water diffusion.

Under initial rate conditions at basic pH, the effect of pre-irradiation is significant but much less pronounced (factor of  $\sim 2$ ). In these conditions, it is accepted that the hydrolysis reaction of Si–O–Si bonds controls the initial dissolution rate of the glass<sup>5,42,53</sup>. The structural analysis of the glass reveals an increase in the fraction of tri-coordinated B and a broadening of the ring size distribution with an increased number of small-sized rings after irradiation (Fig. 1). As

**Fig. 6** | ToF-SIMS profiles for the irradiated sample altered 133 days in the residual rate regime (silica saturated solution, 90°C, pH 9). **a** glass components and hydrogen normalized intensities in Log scale. **b** Au profile showing a maximum implantation depth of 2.2 µm. **c** O isotopic ratio and B profiles plotted in linear scale.  $^{18}\text{O}/^{16}\text{O}$  isotopic ratio of the starting solution 0.096. B retention in the interfacial region of the gel is given by the change slope point marked by the grey arrow (5% of the glass concentration).



the increase of tri-coordinated B increases NBO, thus decreases the degree of polymerization of the silicate network, it should increase the initial dissolution rate. However, according to Kerisit and Pierce (2011), it appears that an increase in the fraction of  $\text{B}^{\text{III}}$  from 52% to 64%, leading to an increase in NBO from 0.037 to 0.1 as in our case, would only result in a few percent impact on the initial dissolution rate<sup>54</sup>. Therefore, this change in the B speciation does not seem capable of explaining alone the measured factor of 2.3 in our experiments. Regarding the medium-range order within the silicate network, it is known that small rings are less stable, thus more prone to dissolve than larger-sized rings<sup>5,55</sup>. Therefore, it is possible that this change in the glass structure explains, at least partly the higher initial dissolution rate of the irradiated glass. This plausible reason is also supported by the fact that complex glass, such as SON68 under alpha

irradiation, does not show a significant increase in the number of small-size rings<sup>35,56</sup> and exhibits no significant variation in the initial dissolution rate regardless of the dose<sup>36</sup>.

Finally, under residual rate conditions achieved by a solution highly enriched in silica, the gels formed on both types of samples exhibit different passivating properties. In previous studies, we established that gels formed on CJ2 and ISG in a silica-saturated solution result from in situ reorganization of the silicate network after the release of B and Na instead of complete dissolution Si and Al and reprecipitation<sup>45,57</sup>. Moreover it was also demonstrated for ISG glass that the hydrolysis of B-O-Si bonds constitutes the reaction controlling the first stage of residual rate, typically when B is released proportionally to square root of time<sup>11</sup>. Caution, this result is not generalizable to all borosilicate glasses and all pH conditions. This mechanism is limiting only if the B content of the glass allows the

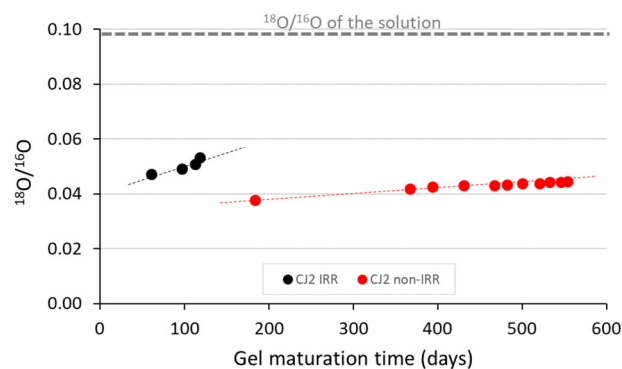


**Fig. 7 | Evolution of the oxygen isotopic ratio within the gel as a function of gel maturation time.** Gel maturation time corresponds to the actual contact duration of the gel with the solution. The calculation was performed by segmenting the gel every 100 or 500 nm based on ICP analyses and determining the oxygen isotopic ratio in each slice from ToF-SIMS analyses (see Supplementary Information 4 for more details).

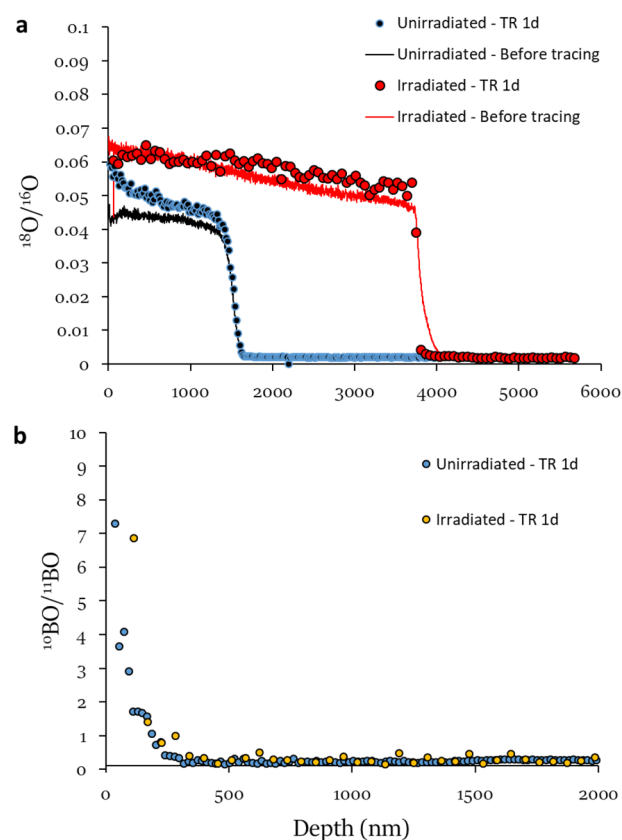


**Fig. 8 | ToF-SIMS profiles obtained after the tracing experiment (1 day at room temperature in the solution spiked with  $^{18}\text{O}$  and  $^{10}\text{B}$ ).** TR stands for tracing experiment. **a**  $^{18}\text{O}/^{16}\text{O}$  profiles in the altered samples and comparison with the same isotopic profiles before the tracing experiment. **b**  $^{10}\text{B}/^{11}\text{B}$  profiles after the 1-day tracing experiment in the two altered samples. BO species were selected rather than B because of a better signal.

percolation of B–O–Si bonds into the network formed by Si–O–Si and Si–O–Al bonds and pH range between 7 and 9<sup>11</sup>. Given that CJ2 glass has the same elemental molar ratios as ISG glass and experiment was carried out at pH 9, such an argument about the rate-limiting reaction is also valid for this glass<sup>58</sup>. These arguments corroborate a former result on the effect of irradiation on CJ2 suggesting that the first gel formed inherits from the glass structure<sup>33</sup>, meaning that the gel formed on irradiated glass is more

disordered than that formed on non-irradiated glass. To go further, one may then wonder why the residual rate of CJ2 glass is less impacted by irradiation than the initial stage of interdiffusion also controlled by B–O–Si bond breaking. Glass passivation by the gel results from hydrolysis and condensation reactions (transformation of silanols into siloxanes), modifying the diffusion of aqueous species into the gel porosity through porosity closure<sup>59–61</sup>. It is undeniable that the structural disorder induced by irradiation increases the glass hydrolysis rate (effect on the initial rate as shown in this study). But it also seems that structural disorder induced by irradiation increases the recondensation rate within the gel structure<sup>33,62</sup>. Thus, the gel of the irradiated glass, which is more disordered than that formed on nonirradiated glass, would form more quickly but also reorganize more rapidly than the gel of the non-irradiated glass. In our study, this is evidenced by a more significant incorporation of  $^{18}\text{O}$  into the gel of the irradiated glass than into the gel of the control glass (Figs. 4, 5, and 7). This is certainly why the effect of irradiation on the glass dissolution rate is less pronounced in residual rate regime than in interdiffusion regime.

Another aspect concerning limiting mechanisms deserves discussion. As mentioned earlier, in interdiffusion and residual regimes, the hydrolysis of B–O–Si bonds constitutes a limiting mechanism, whereas in the initial dissolution regime, the hydrolysis of Si–O–Si bonds controls glass dissolution. How can we explain this change when B seems always easier to dissolve than Si? By basing our reasoning on ISG glass, for which more data is available than for CJ2 glass, in a dilute solution ( $r(\text{Si}) \sim 0$ ), glass dissolution shifts from an incongruent regime in acidic medium ( $r(\text{B}) = r(\text{Na}) \gg r(\text{Si})$ ) to a congruent regime in basic medium ( $r(\text{B}) = r(\text{Na}) = r(\text{Si})$ )<sup>10</sup>. This phenomenon is also observed for the complex glass such as SON68<sup>63</sup>. We interpret this behavior by the preferential attack of Si–O–Si bonds in a basic medium by  $\text{OH}^-$  and the preferential attack of Si–O–B bonds by  $\text{H}_3\text{O}^+$ . When the solution becomes enriched with Si, a so-called saturation effect occurs, meaning that the net Si flux in solution becomes zero<sup>64,65</sup>. In principle, a net zero flux does not necessarily mean that Si does not dissolve; it suffices for the dissolution and precipitation fluxes to be equal. However, alteration experiments conducted in a solution enriched with  $^{29}\text{Si}$  show that when the solution is close to saturation with respect to amorphous silica, gel formation only occurs with silicon from the glass, indicating that the gel does not form by Si dissolution and reprecipitation, and consequently, the Si dissolution flux is very low<sup>45,57,66</sup>. These isotopic experiments demonstrated that the presence of Si in solution significantly decreases the hydrolysis rate of Si–O–Si bonds. Therefore, B can continue to dissolve if there are enough Si–O–B bonds in the glass to percolate into the network formed by Si–O–Si bonds. The glass dissolution rate in this case will increase with the acidity of the solution as shown in a previous study on ISG<sup>11</sup>. If the number of Si–O–B bonds in the glass is below the percolation threshold in the silicate network, then B cannot dissolve in the residual regime. This has recently been observed for a 5-oxide glass called S65.5 with a composition (mol%) of 65.5  $\text{SiO}_2$  9  $\text{B}_2\text{O}_3$  6.8  $\text{Al}_2\text{O}_3$  12.7  $\text{Na}_2\text{O}$  4.1  $\text{CaO}$  ( $\text{B}/(\text{Si}+\text{Al}) = 0.22$  for S65.5 vs. 0.47 for CJ2 or ISG)<sup>67</sup>. Figure 9 summarizes this discussion for CJ2, ISG, and SON68-type glasses.

Regarding the incorporation of  $^{18}\text{O}$  in the gel during the tracing experiment, it can be noted that the gel formed from the irradiated glass incorporates significantly less  $^{18}\text{O}$  than a gel formed on ISG glass irradiated with 1 GeV Xe ions altered under similar conditions<sup>33</sup>. Indeed, in the study on the ISG, the isotopic ratio of  $^{18}\text{O}/^{16}\text{O}$  in the gel after the same 24-hour tracing experiment at room temperature reaches 0.14 in the inner part of the gel, compared to 0.06 in our study. This significant difference could be attributed to the trace formation in the glass structure by high-energy Xe ions, leaving preferential percolation paths in the newly formed gel. This trace formation phenomenon related to the energy of incident ions does not occur for the 7 MeV Au ions used in our study<sup>56</sup>.

In conclusion, this study demonstrates that the structural disorder induced by 7 MeV Au ion irradiation significantly lowers the chemical



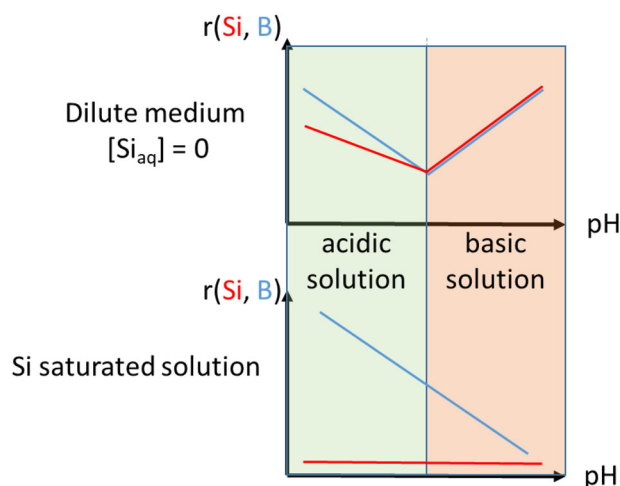


**Fig. 9 | Phenomenology of the dissolution of CJ2, ISG, or SON68 type glasses, far or near saturation, as a function of pH.** This phenomenology is applicable to glasses with a sufficient concentration of B, allowing the percolation of Si–O–B bonds into the network of Si–O–Si bonds. In a dilute basic environment, the initial rate corresponds to the dissolution rate of Si, while in a Si-saturated environment, the residual rate corresponds to the dissolution rate of B.

**Table 1 | Conditions for the residual rate regime experiments**

	Non-Irradiated	Irradiated
T (°C)	90 ± 1	90 ± 1
V (mL)	20.46	23.48
S (cm <sup>2</sup> )	1.73	12.2
S/V (cm <sup>-1</sup> )	0.08	0.52
Mode	Static (no stirring, no solution renewal)	Static (no stirring, no solution renewal)
pH <sup>90°C</sup>	9 ± 0.1	9 ± 0.1
C <sub>0</sub> (Si) (mg.L <sup>-1</sup> )	286 ± 9	257 ± 8
<sup>18</sup> O/ <sup>16</sup> O	0.098 ± 0.005	0.096 ± 0.005
Duration (days)	563	133

durability of CJ2 glass. The impact is particularly pronounced on the interdiffusion mechanism. However, it is less marked on the initial rate regime in a basic environment and on the residual rate regime. We attribute this lesser effect on the residual rate compared to interdiffusion to the fact that the gel formed on the irradiated glass restructures more rapidly than on the non-irradiated glass. This confirms the idea that the impact of structural disorder on the residual dissolution rate of the glass obtained in static mode would be transient. But, in this study, we induced structural disorder before alteration. In the case of nuclear glass, alteration may occur simultaneously with alpha decay-induced disorder. To more accurately assess this situation, it will be necessary to evaluate the dynamics of disorder creation along with the reorganization of the gel to become passive.

## Methods

### Glass preparation

Glass CJ2 (64.9 SiO<sub>2</sub>, 17.3 B<sub>2</sub>O<sub>3</sub>, 13.6 Na<sub>2</sub>O, 4.1 Al<sub>2</sub>O<sub>3</sub> in mol%) was prepared with analytical grade carbonate and oxide powders and melted twice at 1500°C and 1450°C, respectively. After the second batch, the glasses were annealed for 3 h at T<sub>g</sub> + 20 K (530°C). The nominal composition given above was verified by caustic fusion followed by acid dissolution and ICP-OES analyses<sup>30</sup>. The glass has (48 ± 2)% four-fold coordinated B according to NMR<sup>33</sup> leading to a fraction of NBO per tetrahedron of Si+Al of 0.037.

From the bar, monoliths were prepared by cutting and polishing all the faces at various grades up to a diamond suspension of 0.05 μm, leading to the

surface roughness of the order of a few nm. Before use, monoliths were cleaned in acetone and absolute ethanol.

CJ2 glass monoliths were irradiated on both sides with 7 MeV Au<sup>3+</sup> ions on the 2MV Aramis accelerator at the SCALP facility (CNRS-CSNSM, Orsay, France) to induce a significant nuclear damage in the glass structure<sup>56</sup>. A fluence of 2 × 10<sup>14</sup> at.cm<sup>-2</sup> was used, to induces a minimum nuclear dose of around 40 MGy in an irradiated depth of 1.8 μm and thus to reach the saturation damage. The Au implantation profile was measured by negative ions analysis by Time-of-Flight Secondary Ion Mass Spectrometry (ToF-SIMS) and was also obtained by simulation with the Stopping and Range of Ions in Matter (SRIM) software<sup>68</sup>. The comparison given in Supplementary Information 1 shows a good agreement: the 7 MeV Au<sup>3+</sup> ions stop after a range of around 2 μm within the glass, creating thus a damage depth of 1.8–2 μm thick.

### Raman spectroscopy

The pristine and the pre-irradiated glasses were analysed by Raman spectroscopy on a Horiba Jobin Yvon XploRA Plus spectrometer with 1800 g.mm<sup>-1</sup> at the CEA Marcoule laboratory. The spectra were recorded at a 532 nm wavelength perpendicularly to the pristine glass sample surface, focused at the surface and using a confocal hole of 100 μm that allow the characterization of the first 2 microns below the glass surface<sup>69</sup>. For each analysis, 15 accumulations of 240 s were obtained in the exact same condition and position.

### Interdiffusion rate measurement

The interdiffusion experiments were conducted in perfluoroalkoxy (PFA) vessel. For each experiment, 40 mL 18.2 mΩ·cm of deionized water was heated to 30 ± 1°C. The pH<sup>90°C</sup> was adjusted to 1 ± 0.1 with a 1 mol L<sup>-1</sup> HNO<sub>3</sub> solution. Polished glass coupons were cleaned with ethanol then put inside PFA basket so that the glass coupons were positioned at mid-height in the solution. Each reactor (one for non-irradiated glass and the other for irradiated glass) contained two coupons. The first was retrieved after 8 hours, the other after 3 days. When taken out of the solution, a coupon is immediately rinsed with deionized water, then dried at 50°C before storage. At day 3, 2 mL of solution were sampled, then acidified with HNO<sub>3</sub> and analyzed by ICP-OES (Thermo Scientific ICAP 6300 Duo operated at CEA Marcoule) to determine Si, B, Na and Al concentrations.

### Initial dissolution rate measurement

The initial alteration rate experiments were conducted in the PFA vessel. For each experiment, 500 mL 18.2 mΩ·cm of deionized water was heated to 90 ± 1°C. The pH<sup>90°C</sup> was adjusted to 9 ± 0.1 with a 0.1 mol L<sup>-1</sup> LiOH solution. For the irradiated glass, a coupon of 2.375 × 2.358 × 0.094 cm<sup>3</sup> was prepared. Only the two large faces were irradiated. The ratio between the irradiated faces and the 4 non-irradiated faces, *f*, is 0.079. For the non-irradiated glass the experiment was conducted on a 2.378 × 2.359 × 0.095 cm<sup>3</sup> coupon. Prior to the experiment, each coupon was carefully cleaned with ethanol, dried, and put inside a PFA basket.

This basket was then suspended inside the solution vessel using a Teflon tape. To ensure the homogeneity of the solution, a magnetic stirring system was used. In this configuration, the Reynolds number, a dimensionless number indicating the flow pattern, was estimated to be larger than 2000, a value characteristic of a turbulent flow at the glass surface. The whole experiment was conducted in an oven that was maintained at 90 ± 1°C. Two milliliters of solution sample were taken with a syringe at regular time intervals until the end of the experiments (3.3 days for non-irradiated glass and 1.3 days for irradiated glass). The pH and temperature were measured at regular intervals.

Concentrations of the elements in the samplings were determined by ICP-OES (Thermo Scientific ICAP 6300 Duo operated at CEA Marcoule). After correcting the concentrations with the respective factor of dilution, the normalized mass losses in (g·m<sup>-2</sup>) are calculated using the following

**Table 2 | Operating conditions for the ToF-SIMS analyses**

Sample	Abrasion				Analysis				
	Primary ions	E (keV)	I (nA)	Area (μm <sup>2</sup> )	Primary ions	E (keV)	I (pA)	Area (μm <sup>2</sup> )	Secondary ions
<b>Interdiffusion</b>									
8 hr Nlrr	O <sub>2</sub> <sup>+</sup>	0.5	110	350 × 350	Bi <sub>1</sub> <sup>+</sup>	25	1.5	50 × 50	+
8 hr Irr	O <sub>2</sub> <sup>+</sup>	2	789	300 × 300	Bi <sub>1</sub> <sup>+</sup>	25	1.5	50 × 50	+
3d Nlrr	O <sub>2</sub> <sup>+</sup>	1	168	400 × 400	Bi <sub>1</sub> <sup>+</sup>	25	1	50 × 50	+
3d Irr	O <sub>2</sub> <sup>+</sup>	2	988	200 × 200	Bi <sub>1</sub> <sup>+</sup>	25	1	50 × 50	+
<b>Residual rate</b>									
563d Nlrr	Cs <sup>+</sup>	2	128	200 × 200	Bi <sub>1</sub> <sup>+</sup>	25	1	50 × 50	-
133d Irr	Cs <sup>+</sup>	2	112	200 × 200	Bi <sub>1</sub> <sup>+</sup>	25	1	50 × 50	-
563d Nlrr – cryo 1d	Cs <sup>+</sup>	2	130	200 × 200	Bi <sub>1</sub> <sup>+</sup>	25	1	50 × 50	-
133d Irr – cryo 1d	Cs <sup>+</sup>	2	130	200 × 200	Bi <sub>1</sub> <sup>+</sup>	25	1	50 × 50	-

Nlrr and Irr stand for nonirradiated samples and irradiated samples, respectively.

equation:

$$NL(i) = 10^{-2} \frac{C(i)V}{SX_i} \quad (1)$$

where  $C(i)$  is the concentration in  $\text{mg}\cdot\text{L}^{-1}$  of element  $i$  in the solution,  $S/V$  is the glass surface area to solution volume ratio ( $\text{cm}^{-1}$ ), and  $X_i$  is the mass fraction of the element in the glass.

From Eq. (1), equivalent thickness of altered glass,  $Eth(i)$ , in  $\mu\text{m}$  of the element dissolved from the glass of density  $\rho_g$  is given by:

$$Eth(i) = \frac{NL(i)}{\rho_g} \quad (2)$$

The initial rate,  $r_0$ , in  $\text{g}\cdot\text{m}^{-2}\cdot\text{d}^{-1}$  is given by:

$$r_0 = \frac{d(NL(i))}{dt} \quad (3)$$

Making sure that (i) the solution remains diluted to prevent feedback reactions, (ii)  $i$  is a glass dissolution tracer, (iii) glass dissolution is linear and congruent. Uncertainty on  $r_0$  is  $\pm 30\%$  according to a previous study conducted in similar conditions<sup>43</sup>.

The initial dissolution rate of irradiated glass,  $r_{0,irr}$ , was corrected to account for the small unirradiated faces of the coupon according to the following formula:

$$\text{Corrected } r_{0,irr} = \frac{r_{0,irr} - f \cdot r_{0,non-irr}}{1 - f} \quad (4)$$

Where  $f$  is  $S_{non-irr}/S_{total}$ .

### Residual rate measurement

Experiments focusing on residual rate conditions were carried out in static mode using a PFA vessel in which polished coupons of CJ2 glass were put in solution enriched in silica (~80% of the saturation with respect to amorphous silica) and <sup>18</sup>O (H<sub>2</sub><sup>18</sup>O from Cortecnet, France). Each vessel contained two glass coupons placed in a Teflon basket. Experimental conditions are listed in Table 1. Note that the glass-surface-area-to-solution-volume ratio,  $S/V$ , differs in the two experiments because of the coupons size, which were different. In the silica-saturated conditions used in these experiments, this parameter has no impact on the glass behavior meaning that the comparison between the two experiments is not biased<sup>57,70</sup>.

At day 133 and day 563 a glass coupon was retrieved from the irradiated CJ2 reactor and non-irradiated CJ2 reactor, respectively.

Coupons were rinsed with deionized water and dried at 50°C temperature. They were then analyzed by ToF-SIMS (see the next section). After analysis they were immersed in a so called tracing solution at pH 9 containing  $1\text{ g}\cdot\text{L}^{-1}$  of <sup>10</sup>B and <sup>18</sup>O (H<sub>2</sub><sup>18</sup>O from Cortecnet, France, H<sub>3</sub><sup>10</sup>BO<sub>3</sub> 99% <sup>10</sup>B from Aldrich). This tracing experiment was conducted for 24 hours at room temperature. After taken out a residual film of solution remained on the glass surface. It was removed by blowing dry air before the coupons were plunged in liquid N<sub>2</sub> for 10 min. A ToF-SIMS analysis was then performed keeping the sample cold (down to -150°C) to prevent pore water evaporation during analysis (cryo mode)<sup>37</sup>.

### ToF-SIMS analyses

ToF-SIMS analyses were carried out by Tescan Analytix in Fuveau (France) on a TOF 5 device from IONTOF. Analyses were performed in abrasion-analysis mode according to the conditions listed in Table 2.

Neutralisation of the surface charge was performed by a pulsed flux of low-energy electrons (< 20 eV). The depth calibrations were carried out by measuring the size of the craters with a 1D mechanical profilometer.

For each element, point-to-point intensity at each step was divided by the mean point-to-point intensity recorded in the pristine glass, giving normalized intensities. Isotopic ratios (e.g. <sup>18</sup>O/<sup>16</sup>O, <sup>10</sup>BO/<sup>11</sup>BO) were obtained by dividing point-to-point intensities at each depth. The mean value in the pristine glass was compared to natural abundance. The observed deviation varied from a few percent to a few tens of percent. A proportional correction has been applied to the entire curve in order to set the value in pristine glass to the natural abundance.

See Collin et al.<sup>37</sup> for more details on the use of ToF-SIMS for gel characterization.

### Data availability

The data that support the findings of this study are available from the corresponding authors on reasonable request.

Received: 21 February 2024; Accepted: 31 May 2024;

Published online: 17 June 2024

### References

- Ojovan, M. I. & Lee, W. E. Glassy Wasteforms for Nuclear Waste Immobilization. *Metall. Mater. Trans. A-Phys. Metall. Mater. Sci.* **42A**, 837–851 (2011).
- Gin, S., Jollivet, P., Tribet, M., Peugeot, S. & Schuller, S. Radionuclides containment in nuclear glasses: an overview. *Radiochim. Acta* **105**, 927–959 (2017).

3. Donald, I. W., Metcalfe, B. L. & Taylor, R. N. J. The immobilization of high level radioactive wastes using ceramics and glasses. *J. Mater. Sci.* **32**, 5851–5887 (1997).
4. Vienna, J. D., Ryan, J. V., Gin, S. & Inagaki, Y. Current Understanding and Remaining Challenges in Modeling Long-Term Degradation of Borosilicate Nuclear Waste Glasses. *Int. J. Appl. Glass Sci.* **4**, 283–294 (2013).
5. Bunker, B. C. Molecular mechanisms for corrosion of silica and silicate-glasses. *J. Non-Cryst. Solids* **179**, 300–308 (1994).
6. Frankel, G. S. et al. Recent Advances in Corrosion Science Applicable To Disposal of High-Level Nuclear Waste. *Chem. Rev.* **121**, 12327–12383 (2021).
7. Gin, S., Delaye, J.-M., Angeli, F. & Schuller, S. Aqueous alteration of silicate glass: state of knowledge and perspectives. *npj Mater. Degrad.* **5**, 42 (2021).
8. Gin, S. et al. The fate of silicon during glass corrosion under alkaline conditions: a mechanistic and kinetic study with the International Simple Glass. *Geochim. Cosmochim. Acta* **151**, 68–85 (2015).
9. Frugier, P. et al. SON68 nuclear glass dissolution kinetics: current state of knowledge and basis of the new GRAAL model. *J. Nucl. Mater.* **380**, 8–21 (2008).
10. Inagaki, Y., Kikunaga, T., Idemitsu, K. & Arima, T. Initial Dissolution Rate of the International Simple Glass as a Function of pH and Temperature Measured Using Microchannel Flow-Through Test Method. *Int. J. Appl. Glass Sci.* **4**, 317–327 (2013).
11. Gin, S. et al. Insights into the mechanisms controlling the residual corrosion rate of borosilicate glasses. *Npj Materials Degradation* **4**, <https://doi.org/10.1038/s41529-020-00145-2> (2020).
12. Strachan, D. et al. On the dissolution of a borosilicate glass with the use of isotopic tracing - Insights into the mechanism for the long-term dissolution rate. *Geochim. Cosmochim. Acta* **318**, 213–229 (2022).
13. Kumar, R., Jan, A., Bauchy, M. & Krishnan, N. M. A. Effect of irradiation on the atomic structure of borosilicate glasses. *J. Am. Ceram. Soc.* **104**, 6194–6206 (2021).
14. Peugeot, S. et al. Effect of alpha radiation on the leaching behaviour of nuclear glass. *J. Nucl. Mater.* **362**, 474–479 (2007).
15. Weber, W. J. et al. Radiation effects in glasses used for immobilization of high-level waste and plutonium disposition. *J. Mater. Res.* **12**, 1946–1978 (1997).
16. Peugeot, S. et al. Irradiation stability of R7T7-type borosilicate glass. *J. Nucl. Mater.* **354**, 1–13 (2006).
17. Delaye, J. M. et al. Investigation of alumino-silicate glasses by coupling experiments and simulations: Part II-radiation effects. *J. Non-Cryst Solids* **569**, <https://doi.org/10.1016/j.jnoncrysol.2021.120969> (2021).
18. Mendoza, C. et al. Oxide glass structure evolution under swift heavy ion irradiation. *Nucl. Instrum. Methods Phys. Res. Sect. B-Beam Interact. Mater. At.* **325**, 54–65 (2014).
19. Mir, A. H. & Peugeot, S. Using external ion irradiations for simulating self-irradiation damage in nuclear waste glasses: State of the art, recommendations and prospects. *J. Nuclear Mater.* **539**, <https://doi.org/10.1016/j.jnucmat.2020.152246> (2020).
20. Ojovan, M. I. & Lee, W. E. in *Symposium on Radiation Effects and Ion-Beam Processing of Materials held at the 2003 MRS Fall Meeting*. 75–80.
21. Lonartz, M. I. et al. The Effect of Heavy Ion Irradiation on the Forward Dissolution Rate of Borosilicate Glasses Studied In Situ and Real Time by Fluid-Cell Raman Spectroscopy. *Materials* **12**, 13 (2019).
22. Weber, W. J., Wald, J. W. & McVay, G. L. Effects of alpha-radiolysis on leaching of a nuclear waste glass. *J. Am. Ceram. Soc.* **68**, C253–C255 (1985).
23. Zhang, H. et al. Effects of vapor hydration and radiation on the leaching behavior of nuclear glass. *J. Nuclear Mater.* **578**, <https://doi.org/10.1016/j.jnucmat.2023.154368> (2023).
24. Gillet, C., Szenknect, S., Tribet, M., Arena, H. & Peugeot, S. Impact of gold ion irradiation on the initial alteration rate of the International Simple Glass. *J. Nucl. Mater.* **588**, 154817 (2024).
25. Wellman, D. M., Icenhower, J. P. & Weber, W. J. Elemental dissolution study of Pu-bearing borosilicate glasses. *J. Nucl. Mater.* **340**, 149–162 (2005).
26. Peugeot, S., Tribet, M., Mougnaud, S., Miro, S. & Jegou, C. Radiations effects in ISG glass: from structural changes to long-term aqueous behavior. *Npj Mater. Degradat.* **2**, <https://doi.org/10.1038/s41529-018-0044-3> (2018).
27. Tribet, M. et al. Alpha dose rate and decay dose impacts on the long-term alteration of HLW nuclear glasses. *npj Mater. Degrad.* **5**, 36, <https://doi.org/10.1038/s41529-021-00183-4> (2021).
28. Angeli, F. et al. Effect of thermally induced structural disorder on the chemical durability of International Simple Glass. *Npj Mater. Degradat.* **2**, <https://doi.org/10.1038/s41529-018-0052-3> (2018).
29. Gin, S. et al. An international initiative on long-term behavior of high-level nuclear waste glass. *Mater. Today* **16**, 243–248 (2013).
30. Gin, S., Beaudoux, X., Angeli, F., Jegou, C. & Godon, N. Effect of composition on the short-term and long-term dissolution rates of ten borosilicate glasses of increasing complexity from 3 to 30 oxides. *J. Non-Cryst. Solids* **358**, 2559–2570 (2012).
31. Boizot, B., Petite, G., Ghaleb, D., Reynard, B. & Calas, G. Raman study of  $\beta$ -irradiated glasses. *J. Non-Cryst. Solids* **243**, 268–272 (1999).
32. Mir, A. H., Monnet, I., Boizot, B., Jégou, C. & Peugeot, S. Electron and electron-ion sequential irradiation of borosilicate glasses: Impact of the pre-existing defects. *J. Nucl. Mater.* **489**, 91–98 (2017).
33. Gin, S. et al. Effects of irradiation on the mechanisms controlling the residual rate of an alumino-borosilicate glass. *Npj Materials Degradation* **6**, <https://doi.org/10.1038/s41529-022-00266-w> (2022).
34. Karakurt, G. et al. Understanding of the mechanical and structural changes induced by alpha particles and heavy ions in the French simulated nuclear waste glass. *J. Nucl. Mater.* **475**, 243–254 (2016).
35. Peugeot, S. et al. in *2nd International Summer School on Nuclear Glass Wasteform - Structure, Properties and Long-Term Behavior (SumGLASS)*. 252–261.
36. Peugeot, S., Delaye, J. M. & Jégou, C. Specific outcomes of the research on the radiation stability of the French nuclear glass towards alpha decay accumulation. *J. Nucl. Mater.* **444**, 76–91 (2014).
37. Collin, M. et al. ToF-SIMS depth profiling of altered glass. *Npj Mater. Degradat.* **3**, <https://doi.org/10.1038/s41529-019-0076-3> (2019).
38. Collin, M., Fournier, M., Charpentier, T., Moskura, M. & Gin, S. Impact of alkali on the passivation of silicate glass. *Npj Materials Degradation* **2**, <https://doi.org/10.1038/s41529-018-0036-3> (2018).
39. Deng, L. et al. Ion-exchange mechanisms and interfacial reaction kinetics during aqueous corrosion of sodium silicate glasses. *npj Mater. Degrad.* **5**, 15, <https://doi.org/10.1038/s41529-021-00159-4> (2021).
40. Bunker, B. C., Arnold, G. W., Day, D. E. & Bray, P. J. The effect of molecular-structure on borosilicate glass leaching. *J. Non-Cryst. Solids* **87**, 226–253, [https://doi.org/10.1016/s0022-3093\(86\)80080-1](https://doi.org/10.1016/s0022-3093(86)80080-1) (1986).
41. Le Losq, C. et al. Percolation channels: a universal idea to describe the atomic structure and dynamics of glasses and melts. *Sci. Rep.* **7**, 16490, <https://doi.org/10.1038/s41598-017-16741-3> (2017).
42. Gin, S. et al. Can a simple topological-constraints-based model predict the initial dissolution rate of borosilicate and aluminosilicate glasses? *Npj Mater. Degradat.* **4**, <https://doi.org/10.1038/s41529-020-0111-4> (2020).
43. Fournier, M. et al. Glass dissolution rate measurement and calculation revisited. *J. Nucl. Mater.* **476**, 140–154 (2016).
44. Jan, A. et al. Radiation effects on the structure and alteration behavior of an  $\text{SiO}_2\text{-Al}_2\text{O}_3\text{-B}_2\text{O}_3\text{-Na}_2\text{O}$  glass. *Int. J. Appl. Glass Sci.* **14**, 113–132 (2023).

45. Gin, S. et al. A General Mechanism for Gel Layer Formation on Borosilicate Glass under Aqueous Corrosion. *J. Phys. Chem. C*. **124**, 5132–5144 (2020).
46. Mir, A. H. et al. Effect of decades of corrosion on the microstructure of altered glasses and their radiation stability. *Npj Mater. Degradat.* **4**, <https://doi.org/10.1038/s41529-020-0115-0> (2020).
47. Kaya, H. et al. Estimating Internal Stress of an Alteration Layer Formed on Corroded Boroaluminosilicate Glass through Spectroscopic Ellipsometry Analysis. *Acs Appl. Mater. Interfaces* **13**, 50470–50480 (2021).
48. Damodaran, K., Gin, S., De Montgolfier, J. V., Jegou, C. & Delaye, J. M. Behavior of B in passivating gels formed on International Simple Glass in acid and basic pH. *J. Non-Crystalline Solids* **598**, <https://doi.org/10.1016/j.jnoncrysol.2022.121938> (2022).
49. Kaya, H., Gin, S., Vogt, B. D. & Kim, S. H. Impact of aqueous solution pH on network structure of corrosion-induced surface layers of boroaluminosilicate glass. *J. Am. Ceram. Soc.* **105**, 6581–6592 (2022).
50. Jan, A., Delaye, J.-M., Gin, S. & Kerisit, S. Molecular dynamics simulation of ballistic effects in simplified nuclear waste glasses. *J. Non-Cryst. Solids* **505**, 188–201 (2019).
51. Dersch, O., Zouine, A., Rauch, F. & Arai, E. In *Materials Science Applications of Ion Beam Techniques* 248–2 *Materials Science Forum* (eds A. G. Balogh & G. Walter) 389–393 (1997).
52. Aréna, H. et al. Characterization of the boron profile and coordination in altered glass layers by EEL spectroscopy. *Micron* **141**, 102983 (2021).
53. Icenhower, J. P. et al. Experimentally determined dissolution kinetics of Na-rich borosilicate glass at far from equilibrium conditions: Implications for Transition State Theory. *Geochim. Cosmochim. Acta* **72**, 2767–2788 (2008).
54. Kerisit, S. & Pierce, E. M. Monte Carlo simulations of the dissolution of borosilicate and aluminoborosilicate glasses in dilute aqueous solutions. *Geochim. Cosmochim. Acta* **75**, 5296–5309 (2011).
55. Shi, Y. et al. Revealing the relationship between liquid fragility and medium-range order in silicate glasses. *Nat. Commun.* **14**, 13 (2023).
56. Mir, A. H. & Peugeot, S. Using external ion irradiations for simulating self-irradiation damage in nuclear waste glasses: State of the art, recommendations and, prospects. *J. Nucl. Mater.* **539**, 30 (2020).
57. Gin, S. et al. Origin and consequences of silicate glass passivation by surface layers. *Nat. Commun.* **6**, 8 (2015).
58. Lu, X. N., Ren, M. G., Deng, L., Benmore, C. J. & Du, J. C. Structural features of ISG borosilicate nuclear waste glasses revealed from high-energy X-ray diffraction and molecular dynamics simulations. *J. Nucl. Mater.* **515**, 284–293 (2019).
59. Cailleteau, C. et al. Insight into silicate-glass corrosion mechanisms. *Nat. Mater.* **7**, 978–983 (2008).
60. Gin, S. et al. Dynamics of self-reorganization explains passivation of silicate glasses. *Nat. Commun.* **9**, 2169 (2018).
61. Jollivet, P. et al. Investigation of gel porosity clogging during glass leaching. *J. Non-Cryst. Solids* **354**, 4952–4958 (2008).
62. Tribet, M. et al. New Insights about the Importance of the Alteration Layer/Glass Interface. *J. Phys. Chem. C*. **124**, 10032–10044 (2020).
63. Advocat, T., Crovisier, J. L., Vernaz, E., Ehret, G. & Charpentier, H. in *14th International Symp on the Scientific Basis for Nuclear Waste Manage.* 57–64.
64. Neeway, J., Abdelouas, A., Grambow, B. & Schumacher, S. Dissolution mechanism of the SON68 reference nuclear waste glass: New data in dynamic system in silica saturation conditions. *J. Nucl. Mater.* **415**, 31–37 (2011).
65. Icenhower, J. P. & Steefel, C. I. Experimentally determined dissolution kinetics of SON68 glass at 90 °C over a silica saturation interval: Evidence against a linear rate law. *J. Nucl. Mater.* **439**, 137–147 (2013).
66. Collin, M. et al. Structure of International Simple Glass and properties of passivating layer formed in circumneutral pH conditions. *Npj Mater. Degradat.* **2**, <https://doi.org/10.1038/s41529-017-0025-y> (2018).
67. Taron, M. *Simulation du transport réactif à l'échelle nanoscopique : application à la dissolution des verres nucléaires* PhD thesis, University of Montpellier, France, (2022).
68. Ziegler, J. F., Ziegler, M. D. & Biersack, J. P. SRIM – The stopping and range of ions in matter (2010). *Nucl. Instrum. Methods Phys. Res. Sect. B: Beam Interact. Mater. At.* **268**, 1818–1823 (2010).
69. Gillet, C. et al. Impact of complex irradiation scenarios on the structure and the properties of the International Simple Glass. *J. Nucl. Mater.* **572**, 154079 (2022).
70. Gin, S., Frugier, P., Jollivet, P., Bruguier, F. & Curti, E. New Insight into the Residual Rate of Borosilicate Glasses: Effect of S/V and Glass Composition. *Int. J. Appl. Glass Sci.* **4**, 371–382 (2013).

## Acknowledgements

This study was supported by CEA, Orano and EDF. Authors are grateful to Géraldine Parisot from CEA for ICP-OES analyses, Manon Thomas from CEA for initial dissolution rate measurements and Florian Cousy (Tescan Analytics, France) for ToF-SIMS analyses.

## Author contributions

S.G. supervised the study and wrote the paper. All the authors participated to the scientific discussion and contributed to the editing of the manuscript under its present form.

## Competing interests

The authors declare no competing interests.

## Additional information

**Supplementary information** The online version contains supplementary material available at <https://doi.org/10.1038/s41529-024-00483-5>.

**Correspondence** and requests for materials should be addressed to Stéphane Gin.

**Reprints and permissions information** is available at <http://www.nature.com/reprints>

**Publisher's note** Springer Nature remains neutral with regard to jurisdictional claims in published maps and institutional affiliations.

**Open Access** This article is licensed under a Creative Commons Attribution 4.0 International License, which permits use, sharing, adaptation, distribution and reproduction in any medium or format, as long as you give appropriate credit to the original author(s) and the source, provide a link to the Creative Commons licence, and indicate if changes were made. The images or other third party material in this article are included in the article's Creative Commons licence, unless indicated otherwise in a credit line to the material. If material is not included in the article's Creative Commons licence and your intended use is not permitted by statutory regulation or exceeds the permitted use, you will need to obtain permission directly from the copyright holder. To view a copy of this licence, visit <http://creativecommons.org/licenses/by/4.0/>.

© The Author(s) 2024